Control and Cybernetics

vol. **41** (2012) No. 2

An elbow planar manipulator driven by induction motors using sliding mode control for current loop*

by

Eber de C. Diniz, Antonio B.S. Júnior, Dalton A. Honório, Luiz H.S.C. Barreto, Laurinda L. N. dos Reis

Federal University of Ceará
Department of Electrical Engineering
Fortaleza-CE, 60.455-760, Brazil
email: eber@ufc.br

Abstract: The control of a planar elbow manipulator driven by a squirrel-cage induction motor using sliding mode control (SMC) is presented in this paper. The modeling of the manipulator mechanical coupling as a load applied to the induction motor shaft is developed. This has direct influence on both dq currents, which are chosen as the sliding manifold instead of controlling both mechanical and electrical parts as individual processes like most industrial manipulators do. Conventional proportional-integral (PI) controllers are used for each loop, implying easy design procedure and implementation with low computational effort. The system can then be implemented by using a digital signal processor (DSP) and applied in industrial environments. Simulation and experimental results on a real manipulator are shown to validate the proposed control scheme. The results show that there is low steady-state error for the manipulator position.

Keywords: sliding mode control, induction motor drives, manipulators, digital signal processor, PI controllers.

1. Introduction

Most robots use direct current (DC) or permanent magnet synchronous motors, making the manipulator's maintenance more expensive compared to the induction motor counterparts, due to the relatively high cost of the rare-earth magnets used in permanent magnet synchronous machines (Jussi, 2006) or complexity of the DC motor. This is the main reason for replacing them with squirrel-cage

*Submitted: March 2011; Accepted: March 2012

induction motors whenever possible. In this case, Sliding Mode Control (SMC) becomes a nonlinear approach to control induction motors at high performance.

Since DC motors require maintenance more often than their AC counterparts, the adoption of induction motors is of great interest. However, many applications are dominated by DC drives and do not present good performance when using induction motor drives with constant volt/hertz (v/f) scheme. In order to overcome such problem, vector control has been used for the last two decades in the control of AC motors (Novotny and Lipo, 1996; Trzynadlowski, 1982; Blaschke, 1971; Casadei, 2002).

The complexity related to field orientation on manipulators comes from the plant modeling for application of adaptive control (Camara et al., 2003). It also concerns the nonlinear mechanical coupling between links (Spong and Vidyasagar, 2004), which is the specific scope of this work. Hence to ensure good dynamic performance, various robust control strategies for induction motor drives have been reported in literature (Gadoue, Giaouris and Finch, 2009; Szabat, Orlowska-Kowalska and Dybkowski, 2009). One particular scheme has drawn special attention of researchers i.e. SMC, mainly due to simple design procedure, fast dynamic response, easy implementation, and good robustness in face of parameter variations and also load disturbances (Shiau and Lin, 2001; Chan and Wang, 1996), thus showing improved performance over the vector control scheme (Eber et al., 2010a). However, all of the aforementioned schemes have only been used to control a stand-alone induction motor.

The main complexity regarding the control of robot manipulators lies in determining the time history of joint inputs required to cause the end effector to execute a commanded motion. The joint inputs could be joint forces and torques, or they could be inputs to the actuators, as in the case of induction motors. Therefore, one must develop a control scheme able to compensate the mechanical coupling influence on joints and consider this in the control action. There are many applications that use induction motors nowadays, e.g. elevators (Osama and Abdul-Azim, 2008) robots and servo drives (Huh and Bien 2007; Lin, Huang and Chou, 2007; Kumar, Gupta and Bhangale, 2009), where fast control over the torque and position of the motor is mandatory. However, reports on manipulators with two or more degrees of freedom (DOF) using induction motors are basically restricted to simulation results only (Casadei et al., 2002; Camara et al., 2003; Gadoue et al., 2009). Within context, this paper proposes a simplified control of an elbow planar manipulator using squirrel-cage induction motors by modeling the disturbance load and developing an SMC scheme for current tracking to compensate the mechanical coupling. For this purpose, the mechanical coupling has been determined for the specific case of the manipulator and then interpreted as a mechanical load at the induction motor shaft in the system modeling. A conventional PI controller was used for position and speed loop using modified Ziegler-Nichols method for tuning (Astrom et

al., 1995). DSP TMS320F2812 is used in the experimental evaluation, thus enabling enhanced performance of the real-time algorithm and cost-effective design of intelligent controllers for induction motors. This implementation has also shown improved results if compared to the same case study using vector control in an induction motor drive (Diniz et al., 2010b).

2. Dynamic modeling of the induction motor

The block diagram of the indirect field-oriented induction motor drive is shown in Fig. 1. The arrangement consists of an induction servo motor; a current ramp for comparison to drive the Space Vector Pulse Width Modulation (SVPWM) inverter, which has better performance than hysteresis based inverter (Holtz, 1994); a field orientation mechanism; a coordinate translator; an inner speed control loop; and an outer position control loop.

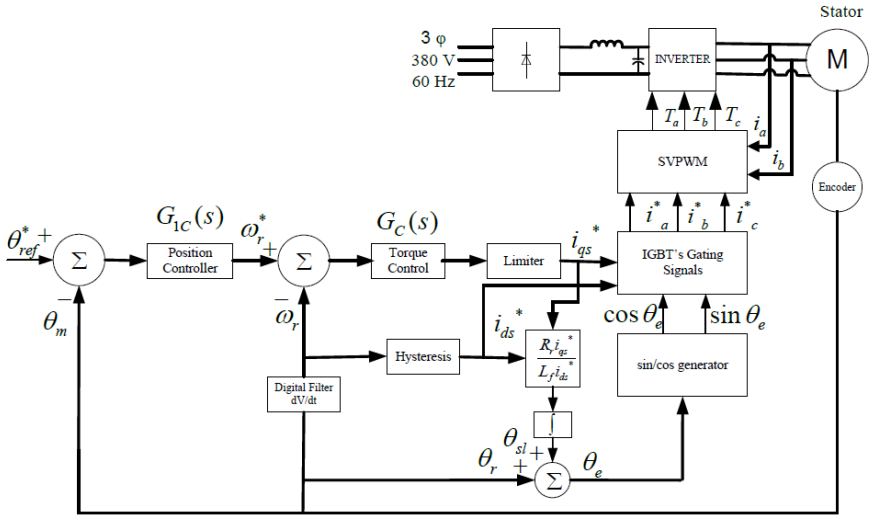

Figure 1. Block diagram representing field-oriented induction motor drive

The state equations of the induction motor in the synchronously rotating reference frame, considered here, can be described by the following relations (Bose, Knoxville, 2001):

$$\frac{d}{dt}\begin{bmatrix} i_{ds} \\ i_{qs} \\ \lambda_{dr} \\ \lambda_{qr} \end{bmatrix} = \tag{1}$$

$$\begin{bmatrix} -\frac{R_s}{\sigma L_s} - \frac{R_r(1-\sigma)}{\sigma L_r} & \omega_e & \frac{L_m R_r}{\sigma L_s L_r^2} & \frac{P\omega_r L_m}{2\sigma L_s L_r^2} \\ \omega_e & -\frac{R_s}{\sigma L_s} - \frac{R_r(1-\sigma)}{\sigma L_r} & -\frac{P\omega_r L_m}{2\sigma L_s L_r^2} & \frac{L_m R_r}{\sigma L_s L_r^2} \\ \frac{L_m R_r}{L_r} & 0 & -\frac{L_r}{R_r} & \omega_e - \frac{P}{2}\omega_r \\ 0 & \frac{L_m R_r}{L_r} & -\left(\omega_e - \frac{P}{2}\omega_r\right) & -\frac{R_r}{L_r} \end{bmatrix} \begin{bmatrix} i_{ds} \\ i_{qs} \\ \lambda_{dr} \\ \lambda_{qr} \end{bmatrix} + \frac{1}{\sigma L_s}\begin{bmatrix} v_{ds} \\ v_{qs} \\ 0 \\ 0 \end{bmatrix}$$

$$T_e = \frac{3PL_m}{4L_r}\left(i_{qs}\lambda_{dr} - i_{ds}\lambda_{qr}\right) \tag{2}$$

where:

T_e - electromagnetic torque;
R_s - stator resistance per phase;
L_s - stator magnetizing inductance per phase;
R_r - rotor resistance per phase referred to the stator;
L_r - rotor magnetizing inductance per phase referred to the stator;
L_m - magnetizing inductance per phase;
P - number of poles;
ω_e - electrical angular speed;
ω_r - slip angular speed;
v_{ds} - d-axis stator voltage;
v_{qs} - q-axis stator voltage;
i_{ds} - d-axis stator current;
i_{qs} - q-axis stator current.

and

$$\begin{aligned} \sigma &= 1 - \frac{L_m^2}{L_s L_r}; \\ \lambda_{qr} &= L_m i_{qs} + L_r i_{dr}; \\ \lambda_{dr} &= L_m i_{ds} + L_r i_{qr}. \end{aligned}$$

In an ideal field-orientated induction motor, decoupling between d and q-axis can be achieved, while the total rotor flux linkage is forced to align with the

d-axis (Novotny and Lipo, 1996). Accordingly, the flux linkage and its derivative in the q-axis are set to zero as:

$$\lambda_{qr} = 0 \quad \text{and} \quad \frac{d\lambda_{qr}}{dt} = 0. \tag{3}$$

The rotor flux linkage can be found from the third row in (1) and by using (3) as:

$$\lambda_{dr} = \frac{L_m i_{ds}}{1 + s\frac{L_r}{R_r}} \tag{4}$$

Compared with the time constant of the mechanical system, the time constant in (4) is assumed to be negligible and i_{ds} is constant ($i_{ds} = i^*_{ds}$) for the desired constant rated rotor flux. Then, expression (4) becomes:

$$\lambda_{dr} = L_m i^*_{ds}. \tag{5}$$

From (3) and (5), the torque (2) is simplified to:

$$T_e = \frac{3PL_m^2}{4L_r} i^*_{ds} i^*_{qs}, \tag{6}$$

where i^*_{qs} denotes the torque current command generated from the torque controller $G_c(s)$. When using indirect field orientation, the slip angular speed is necessary to calculate the unit vector for coordinate translation. By employing the fourth row of (1) and also (3), the slip angular frequency ω_{sl} can be estimated as:

$$\omega_{sl} = \frac{L_m R_r I^*_{qs}}{L_r \lambda_{dr}} = \frac{R_r i^*_{qs}}{L_r i^*_{ds}}. \tag{7}$$

The generated torque, rotor speed ω_r , and rotor angular position θ_r are related by:

$$\omega_r = s\theta_r = \frac{1/J}{s + (B/J)} \left[T_e(s) - T_L(s)\right] \tag{8}$$

where:

B - viscous damping frequency;

J - inertia constant;

T_L - load torque applied to the shaft.

The main problem when vector control algorithms are implemented in DSPs lies in the conversion of the current command represented in (5) and (6) into voltage command (Novotny and Lipo, 1996). To accomplish this task, it is necessary to decouple the voltage equation enabling independent control of the two stator current components in $dq0$ frame (Trzynadlowski, 1982).

This procedure is detailed in Chan and Wang (1996), giving:

$$v_{qs}^{e} = (r_s + L_s^{'}s)i_{qs}^{e} + \omega_e L_s i_{ds}^{e} \tag{9}$$

$$v_{ds}^{e} = r_s i_{ds}^{e} - \omega_e L_s^{'} i_{qs}^{e} \tag{10}$$

where:

$$L_s^{'} = L_s - \frac{L_m^2}{L_r} \tag{11}$$

while the superscript e refers to the electrical reference.

3. Modeling the nonlinear mechanical coupling as a disturbance

For applications that do not involve very fast motion, especially in robots with large gear reduction among the actuators and the links, the independent position control for each joint works satisfactorily.

For the following discussion, let us assume for simplicity that:

$$q_k = \theta_{sk} = r\theta_{mk} \tag{12}$$

where:

θ_{sk} - shaft angular position;

$r\theta_{mk}$ - link angular position with r being the gear ratio.

Then the motion equations for the manipulator, known as Euler-Lagrange equations, can be written as (Spong and Vidyasagar, 2004):

$$\sum_{j=1}^{n} d_{kj}(q)\ddot{q_j} + \sum_{i,j=1}^{n} c_{ikj}(q)\dot{q_i}\dot{q_j} + g_k(q) = \tau_k, \ k = 1, \ldots, n \tag{13}$$

where τ_k is the torque for link k. Equation (13) represents nonlinear inertial, centripetal, *Coriolis*, and gravitational coupling effects due to the motion of the manipulator. For the manipulator shown in Fig. 2, only the second and third joints are of interest, represented by systems $O_1X_1Y_1Z_1$ and $O_2X_2Y_2Z_2$, respectively, because the first one is not affected by coupling effects (Spong and Vidyasagar, 2004).

For a situation where the generalized coordinates are not the joint variables, one must consider a different calculation for the Lagrangian equations (Spong and Vidyasagar, 2004). In the case of the proposed study, one must choose the generalized coordinates as shown in Fig. 3 because angle θ_2 is determined by driving the motor of the second DOF, which is not affected by angle θ_1.

The dynamical equations for this configuration, according to Fig. 3, show that some simplifications are necessary. The following expression then results (Spong and Vidyasagar, 2004):

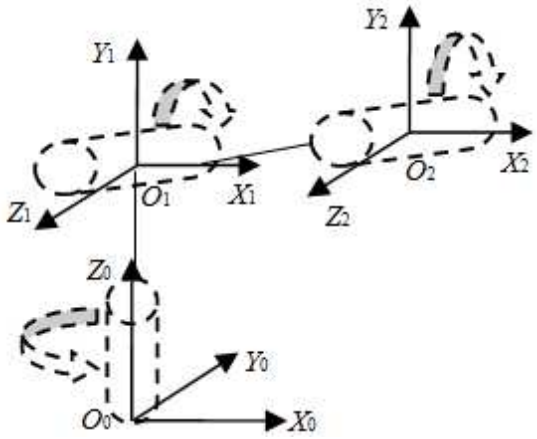

Figure 2. 3-DOF manipulator driven by squirrel-cage induction motors

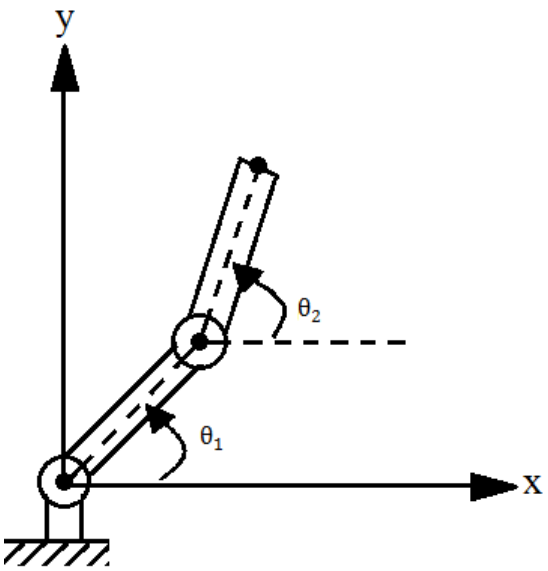

Figure 3. Generalized coordinates for the robot represented in Fig. 2

$$v_{c1} = \begin{bmatrix} -l_{c1}\sin\theta_1 & 0 \\ l_{c1}\cos\theta_1 & 0 \\ 0 & 0 \end{bmatrix} \begin{bmatrix} \dot{\theta_1} \\ \dot{\theta_2} \end{bmatrix} \tag{14}$$

$$v_{c2} = \begin{bmatrix} l_1\sin\theta_1 & -l_{c2}\sin\theta_2 \\ l_1\cos\theta_1 & l_{c2}\cos\theta_2 \\ 0 & 0 \end{bmatrix} \begin{bmatrix} \dot{\theta_1} \\ \dot{\theta_2} \end{bmatrix}$$

where:

l_{cn} - center of mass for link n;
l_n - link size;
k - unit vector in z direction;
v_{ci} - center of mass speed for link i.

The inertial $D(\theta)$ matrix is given by:

$$\begin{bmatrix} m_1 l_{c1}^2 + m_2 l_1^2 + m_1 l_{c1} & m_1 l_1 l_{c2}\cos(theta_2 - theta_1) \\ m_2 l_1 l_{c2}\cos(\theta_2 - \theta_1) & m_2 l_{c2}^2 + m_2 l_{c2} \end{bmatrix} \tag{15}$$

while the Christoffel symbols are defined by (Spong and Vidyasagar, 2004):

$$c_{ijk} = \frac{1}{2}\left\{ \frac{\partial d_{jk}}{\partial q_i} + \frac{\partial d_{ki}}{\partial q_i} - \frac{\partial d_{ij}}{\partial q_k} \right\}. \tag{16}$$

From expression (16) and considering only the last two DOFs, six coefficients can be obtained:

$$\begin{cases} c_{111} = \frac{1}{2}\frac{\partial d_{11}}{\partial \theta_1} = 0 \\ c_{121} = c_{211} = \frac{1}{2}\frac{\partial d_{11}}{\partial \theta_2} = 0 \\ c_{221} = \frac{\partial d_{12}}{\partial \theta_2} - \frac{1}{2}\frac{\partial d_{22}}{\partial \theta_1} = -m_2 l_1 l_{c2}\sin(\theta_2 - \theta_1) \\ c_{112} = \frac{\partial d_{21}}{\partial \theta_1} - \frac{1}{2}\frac{\partial d_{11}}{\partial \theta_2} = m_2 l_1 l_{c2}\sin(\theta_2 - \theta_1) \\ c_{212} = c_{122} = \frac{1}{2}\frac{\partial d_{22}}{\partial \theta_1} = 0 \\ c_{111} = \frac{1}{2}\frac{\partial d_{22}}{\partial \theta_2} = 0. \end{cases} \tag{17}$$

The potential energy of the manipulator P in terms of θ_1 and θ_2 is:

$$P = m_1 glc1\sin\theta_1 + m_2 g(l_1\sin\theta_1 + l_{c2}\sin\theta_2) \tag{18}$$

and the gravitational forces are:

$$g_1 = (m_1 l_{c1} + m_2 l_1) g\cos\theta_1 \tag{19}$$

$$g_1 = m_2 l_{c2} g\cos\theta_2. \tag{20}$$

Finally, the dynamic equations are:

$$d_{11}\ddot{\theta_1} + d_{12}\ddot{\theta_2} + c_{221}\dot{\theta_2}^2 + g_1 = \tau_{L1} \tag{21}$$

$$d_{21}\ddot{\theta_1} + d_{22}\ddot{\theta_2} + c_{112}\dot{\theta_1}^2 + g_2 = \tau_{L2}. \tag{22}$$

4. Sliding mode current control design

The main difficulty in the control of induction motor drives comes from the multiplicative nonlinearity of the developed electromagnetic torque. However, if the current control problem is overcome, speed and position regulation can be easily achieved by outer-loop controllers. For this purpose, the SMC scheme is first applied to the inner-loop current control.

From the SMC point of view, the system trajectories must be required to approach the specified manifold form to any initial state in the state plane. Then the system behavior is governed by the dynamics of the manifold in which the system trajectories remain. Using a proportional controller for position control and a PI for speed control (Shiau and Lin, 2001), as presented in Fig. 4, the reference electromagnetic torque can be described by:

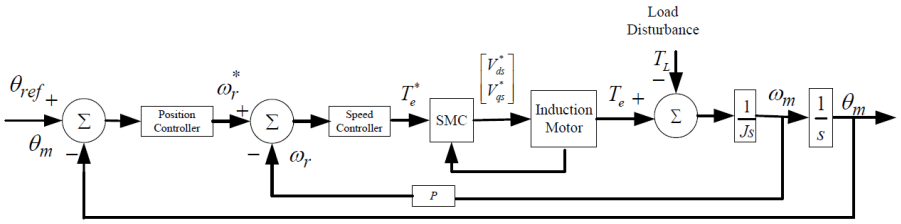

Figure 4. Single induction motor position drive using SMC

$$\omega_r^*(t) = K_{p1}\left[\theta_{ref}(t) - \theta_m(t)\right] \tag{23}$$

$$\begin{aligned} T^* = {} & K_{p2}(\omega_r^* - \omega_r) + K_{i2}(\omega_r^* - \omega_r) = \\ & \frac{PK_{p2}k_T}{J} i_{qs} T_L \lambda_{dr} - \left(\frac{K_{p2} - K_{p1}}{P} + K_{i2}\right)\omega_r - \\ & K_{p1}K_{i2}\theta_m + \frac{PK_{p2}}{J}T_L + K_{p_1}K_{p2}\theta_{ref} + K_{p1}K_{i2}\theta_{ref} \end{aligned} \tag{24}$$

where:

$$k_T = \frac{3P}{4}\frac{L_m}{L_r}. \tag{25}$$

The load torque given in (25) can be replaced by the dynamic equations of both links for joint control i.e. (21) and (22). Also, by using (1) and (7), a twelfth-order state variable dynamic equation for the whole system can be obtained, as seen in Fig. 5.

The torque command is influenced by both quadrature and direct stator currents, according to (4) and (9). It is then reasonable to adopt such currents

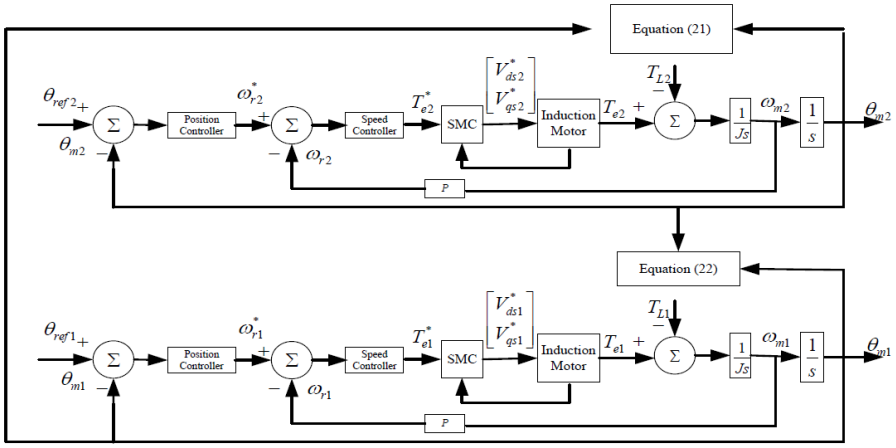

Figure 5. 2-DOF manipulator with induction motor position drive using SMC

as the sliding manifold for the proposed study. The switching function vector for the 2- DOF robot is defined as:

$$s = \begin{bmatrix} s_1 \\ s_2 \\ s_3 \\ s_4 \end{bmatrix} = \begin{bmatrix} i_{ds1} - i^*_{ds1} \\ i_{qs1} - i^*_{qs1} \\ i_{ds2} - i^*_{ds2} \\ i_{qs2} - i^*_{qs2} \end{bmatrix}. \tag{26}$$

From Spong and Vidyasagar (2004), it can be established that the sliding manifold $s = 0$ is globally attractive and an invariant set. The symbol "*" denotes the reference signal, while it is the direct current of the *i-th* DOF and the quadrature current of the *i-th* DOF in $dq0$ reference frame. Keeping the rotoric flux at a constant rate, and using equations (5) and (9), the reference signals are given by:

$$\begin{bmatrix} i^*_{ds1} \\ i^*_{qs1} \\ i^*_{ds2} \\ i^*_{qs2} \end{bmatrix} = \begin{bmatrix} \frac{\lambda_{dr1}}{L_{m1}} \\ \frac{T^*_{e1}}{k_{T1}\lambda_{dr1}} \\ \frac{\lambda_{dr2}}{L_{m2}} \\ \frac{T^*_{e2}}{k_{T2}\lambda_{dr2}} \end{bmatrix}. \tag{27}$$

By using expressions (1), (21), (22), (25), (26), and (27), this gives:

$$s = \begin{bmatrix} a_{11} \\ a_{21} \\ a_{12} \\ a_{22} \end{bmatrix} + \begin{bmatrix} 0 & 0 \\ b_{11} & 0 \\ 0 & 0 \\ 0 & b_{12} \end{bmatrix} \begin{bmatrix} \tau_{L1} \\ \tau_{L2} \end{bmatrix} + \tag{28}$$
$$\begin{bmatrix} 0 & 0 \\ b_{21} & 0 \\ 0 & 0 \\ 0 & b_{22} \end{bmatrix} \begin{bmatrix} \theta_{ref1} \\ \theta_{ref2} \end{bmatrix} +$$
$$\begin{bmatrix} 0 & 0 \\ b_{31} & 0 \\ 0 & 0 \\ 0 & b_{32} \end{bmatrix} \begin{bmatrix} \theta_{ref1} \\ \theta_{ref2} \end{bmatrix} + \frac{1}{\sigma L_s} \begin{bmatrix} v_{ds1} \\ v_{qs1} \\ v_{ds2} \\ v_{qs2} \end{bmatrix}$$

where:

$$a_{1i} = -\frac{1}{\sigma L_{si}} \left(R_{si} + \frac{L_{mi}^2}{\tau_{ri} L_{ri}} \right) i_{dsi} + \frac{L_{mi}}{\tau_r i} \frac{i_{qsi}^2}{\lambda_{dr} i} + \omega_{ri} i_{qsi} + \frac{L_{mi}}{tau_{ri} L_{\sigma i} L_{ri}} \lambda_{dri};$$

$$a_{2i} = -\frac{1}{\sigma L_{si}} \left(R_{si} + \frac{L_{mi}^2}{\tau_{ri} L_{ri}} \right) i_{qsi} - \frac{L_{mi}}{\tau_r i} \frac{i_{qsi} i_{dsi}}{\lambda_{dri}} + \omega_{ri} i_{dsi} + \frac{L_{mi}}{\sigma L_{si} L_{ri}} \lambda_{dri} \omega_{ri}$$
$$- \frac{1}{k_{Ti} \lambda_{dri}} \left(\frac{P_i K_{pi2} k_{Ti}}{J_i} i_{qsi} T_{Li} \lambda_{dri} - \left(\frac{K_{pi2} K_{pi1}}{P_i/2} + K_{ii2} \right) \omega_r - K_{pi1} K_{ii2} \theta_i \right)$$

$$b_{1i} = \frac{\frac{P_i}{2} K_{pi2}}{k_{Ti} \lambda_{dri} J_i}, \quad b_{2i} = -\frac{K_{pi1} K_{pi2}}{k_{Ti} \lambda_{dri}}, \quad b_{3i} = -\frac{K_{pi1} K_{ii2}}{k_{Ti} \lambda_{dri}}. \tag{29}$$

Based on Gao's reaching law design method (Gao and Hung, 1993), a control law for the inner-loop sliding-mode current tracking is proposed as follows:

$$\begin{bmatrix} v_{ds1} \\ v_{qs1} \\ v_{ds2} \\ v_{qs2} \end{bmatrix} = -\sigma L_s \left(\begin{bmatrix} \hat{a}_{11} \\ \hat{a}_{21} \\ \hat{a}_{12} \\ \hat{a}_{22} \end{bmatrix} + \begin{bmatrix} 0 & 0 \\ b_{21} & 0 \\ 0 & 0 \\ 0 & b_{22} \end{bmatrix} \begin{bmatrix} \theta_{ref1} \\ \theta_{ref2} \end{bmatrix} + \right.$$
$$\begin{bmatrix} 0 & 0 \\ b_{31} & 0 \\ 0 & 0 \\ 0 & b_{32} \end{bmatrix} \begin{bmatrix} \theta_{ref1} \\ \theta_{ref2} \end{bmatrix} + \begin{bmatrix} q_1 & 0 & 0 & 0 \\ 0 & q_2 + L_1 & 0 & 0 \\ 0 & 0 & q_3 & 0 \\ 0 & 0 & 0 & q_4 + L_2 \end{bmatrix} sgn(s) +$$
$$\left. \begin{bmatrix} k_1 & 0 & 0 & 0 \\ 0 & k_2 & 0 & 0 \\ 0 & 0 & k_3 & 0 \\ 0 & 0 & 0 & k_4 \end{bmatrix} s \right) \tag{30}$$

where:

$$L_1 = |b_{11}(d_{11}\ddot{\theta}_{max1} + d_{12}\ddot{\theta}_{max2} + c_{221}\dot{\theta}^2_{max2} + g_1)| \quad (31)$$

$$L_2 = |b_{12}(d_{21}\ddot{\theta}_{max1} + d_{22}\ddot{\theta}_{max2} + c_{112}\dot{\theta}^2_{max2} + g_1)| \quad (32)$$

a_{ij} denotes the estimation of a_{ij} and $q_1 > |\hat{a}_{11} - a_{11}|$, $q_2 > |\hat{a}_{21} - a21|$, $q_3 > |\hat{a}_{12} - a_{12}|$, $q_4 > |\hat{a}_{22} - a_{22}|$, $k_1 > 0$, $k_2 > 0$, $k_3 > 0$, $k_4 > 0$, $\ddot{\theta}_{maxi}$ and $\dot{\theta}^2_{maxi}$ are the restrictions for joint acceleration and speed, respectively. With this control law, the sliding manifold $s = 0$ is satisfied. It is important to notice that the derivation of equation (30) comes directly from equations (21) and (22). It ensures that the dynamic behavior of manipulator's torque in each DOF influences the calculation of current commands in the control law stated by equation (30).

The proof of the aforementioned statement is given as follows. Let us consider a scalar Lyapunov function candidate as:

$$V(s) = \frac{1}{2}s^T s = \frac{1}{2}(s_1^2 + s_2^2 + s_3^2 + s_4^2). \quad (33)$$

The derivative of $V(s)$ with the system trajectories based on (33) is given by:

$$\begin{aligned}
\dot{V}(s) &= s_1(a_{11} - \hat{a}_{11}) - s_1 q_1 sgn(s_1) - k_1 s_1^2 + \\
&\quad s_2(a_{21} - \hat{a}_{21}) - s_2 b_{11} T_{L1} - s_2\left[(q_2 - L_1)sgn(s_2) - k_2 s_2^2\right] + \\
&\quad s_3(a_{12} - \hat{a}_{12}) - s_3 q_3 sgn(s_3) - k_3 s_3^2 + s_4(a_{22} - \hat{a}_{22}) - \\
&\quad s_4 b_{21} T_{L2} - s_4\left[(q_4 - L_2)sgn(s_4) - k_4 s_4^2\right] \leq \\
&\quad |s_1||a_{11} - \hat{a}_{11}| - |s_1|q_1 - k_1 s_1^2 + |s_2||a_{21} - \hat{a}_{21}| - |s_2|q_2 - k_2 s_2^2 + \\
&\quad |s_3||a_{12} - \hat{a}_{12}| - |s_3|q_3 - k_3 s_3^2 + |s_4||a_{22} - \hat{a}_{22}| - |s_4|q_4 - k_4 s_4^2 \\
&= -|s_1|(q_1 - |a_{11} - \hat{a}_{11}| - |s_2|(q_2 - |a_{12} - \hat{a}_{12}|) - \\
&\quad |s_3|(q_3 - |a_{21} - \hat{a}_{21}|) - |s_4|(q_4 - |a_{22} - \hat{a}_{22}|) - \\
&\quad (k_1 s_1^2 + k_2 s_2^2 + k_3 s_3^2 + k_4 s_4^2).
\end{aligned} \quad (34)$$

For the aforementioned conditions, a negative derivative results. Therefore, the system trajectories are guaranteed to approach the sliding manifold from any initial state in the state plan (Gao and Hung, 1993). When the system is far from the sliding manifold, this inequality shows that $\dot{V}(s)$ is dominated by $-(k_1 s_1^2 + k_2 s_2^2 + k_3 s_3^2 + k_4 s_4^2)$, because s_i^2 represents the difference between currents, and therefore increments in k_i values cause the reaching time to be reduced. On the other hand, $\dot{V}(s)$ is dominated by $-|s_1|(q_1 - |a_{11} - \hat{a}_{11}|) - |s_2|(q_2 - |a_{12} - \hat{a}_{12}|) - |s_3|(q_3 - |a_{21} - \hat{a}_{21}|) - |s_4|(q_4 - |a_{22} - \hat{a}_{22}|)$ when the current trajectories are close to the sliding manifold, and small values of $(q_i - |a_{ij} - \hat{a}_{ij}|)$

Table 1. **Motor parameters**

Parameters	**Value**
Rated power	0.25 HP
Rated speed	1725 rpm
Rated voltage	220 V
Rated current	1.26 A
Number of poles	4
Rotor resistance referred to the stator	87.44 Ω
Stator resistance	35.58 Ω
Rotor inductance referred to the stator	0.16 H
Stator inductance	0.16 H
Mutual inductance	0.884 H
Inertia moment	$5 \cdot 10^{-4}$ $kg \cdot m^2$
Viscous friction coefficient	$5.65 \cdot 10^{-3}$ $kg \cdot m^2/s$

Table 2. **Manipulator parameters**

Parameters	**Value**
Link II mass	12.45 kg
Link II size	53 cm
Link II distance from center of mass	14.9 cm
Link II moment of inertia	0.43 $kg \cdot m^2$
Link II rotation angle	225^o
Link III mass	5.5 kg
Link III size	37.5 cm
Link III distance from center of mass	10.6 cm
Link III moment of inertia	0.28 $kg \cdot m^2$
Link III rotation angle	300^o

reduce the chattering. As a_{ij} and $\hat{a}_{ij}$ are defined by system parameters and their values do not differ so much from each other, chattering is basically only driven by q_i values.

5. Experimental results

Experimental results on the elbow planar manipulator shown in Fig. 12 are presented giving a low error at steady-state for manipulator position. The induction servo motor used in the drive system is a three-phase deltaconnected, squirrel-cage machine, whose parameters are given in Table 1. The manipulator parameters are shown in Table 2.

In the SMC scheme, the main goal of the proposed controller is fast settling time instead of reduced chattering. The values used for the SMC algorithm

are: $k_1 = 8500$, $k_2 = 5500$, $k_3 = 4500$, $k_4 = 1500$, $q_1 = 300$, $q_2 = 300$, $q_3 = 300$ and $q_4 = 300$. For the position proportional controller and speed PI controller, the calculated parameters observing the desired Nyquist points mentioned in Diniz et al. (2010b) are $K_{p11} = 10.3$, $K_{p21} = 15.5$, $K_{i21} = 5.7$ and $K_{p12} = 7.3$, $K_{p22} = 40.3$, $K_{i22} = 40.0$. The SMC algorithm was implemented on a DSP TMS320F2812 from Texas Instruments® with sample frequency of 2.5 kHz. A DC-AC converter with bootstrap was implemented using SVPWM, with switching frequency of 7.5 kHz. The drive signals for the converter switches are obtained from the DSP. Data was acquired using NI USB- 6009 Data Acquisition® from National®, and later plotted using Scilab®. Fig. 6 and 9 show the link's angular position for the second and third DOFs, respectively. The steady-state errors obtained for position control are 1.3% and 0.6%, being lower than those obtained with vector control algorithm applied to the same manipulator (2.1% and 1.1%, respectively, (Diniz et al., 2010b), as more robust position tracking results in this case.

The q-axis current errors, which are part of the sliding manifold described in equation (26) and represent the machine torque variation, are shown in Figs. 7 and 10. It is worth mentioning that, for the second DOF, the induction motor must drive a reductor and also has the highest load considering all the involved DOFs, consequently leading to high power levels. This can be clearly seen in Fig. 7, where the quadrature current error, which represents the machine torque according to equation (6), is higher for the second link. As the third link has almost no load, the induction motor quadrature current for this DOF is lower than the second DOF counterpart, as seen in Fig. 10. Then a change in quadrature current has greater effect on the direct current waveform depicted in Fig. 8, if compared to the result for the motor in the second link. Since the direct current is driven to a constant value for low speeds, it leads to a major increase in the load, and consequently in the quadrature current. On the other hand, the direct current in the third link is not significantly affected, as shown in Fig. 8. Finally, it is important to state that all currents varied around the sliding manifold $s = 0$ with the chattering controlled by the terms $(q_i - |a)ij - \hat{a}_{ij}|)$ in equation (35), as in Figs. 7, 8, 10, and 11. If compared to the same scheme using vector control to drive the induction motors (Diniz et al., 2010b), it becomes evident that the proposed SMC approach has provided improved performance.

6. Conclusion

This paper has successfully demonstrated the application of a sliding mode current control scheme for an elbow manipulator joint control based on the nonlinear model of induction motors. Parameters for the position and speed controllers such as the manipulator's mechanical coupling are taken into account in the SMC control, offering an intuitive design and implementation with low complexity for practical interest. This allows for tracking the desired trajectory

reference for the motor link coordinates under the assumption that manipulator's mechanical coupling can be modeled and interpreted as a load on the induction motor shaft, thus having direct influence on both direct and quadrature currents. This approach has provided improved results considering the position tracking reference, if compared to the vector control scheme, which has not been implemented considering the mechanical coupling. The SMC algorithm was implemented on a DSP due to low computational effort, enabling its application in industrial environment. The results give low error at steady-state for the manipulator position. The provided simulation and experimental results on the implemented manipulator have then validated the proposed control system.

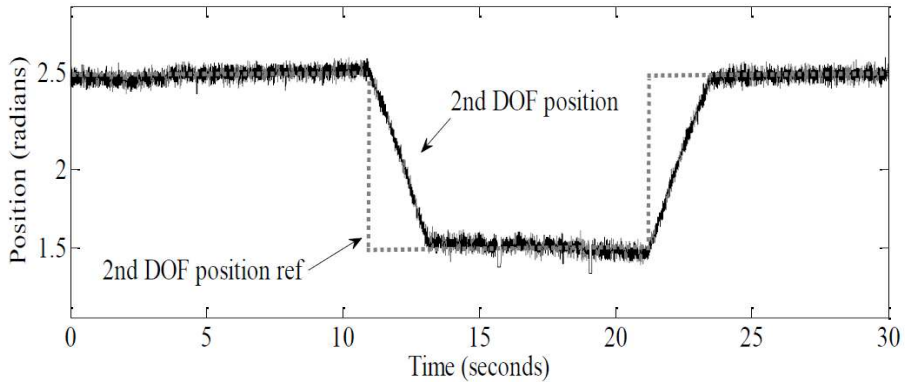

Figure 6. Experimental results of angular position for the 2nd DOF

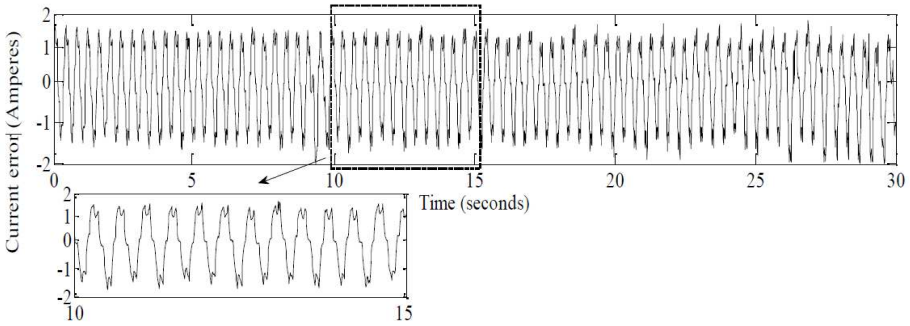

Figure 7. Experimental results of induction motor quadrature current error for the 2nd DOF

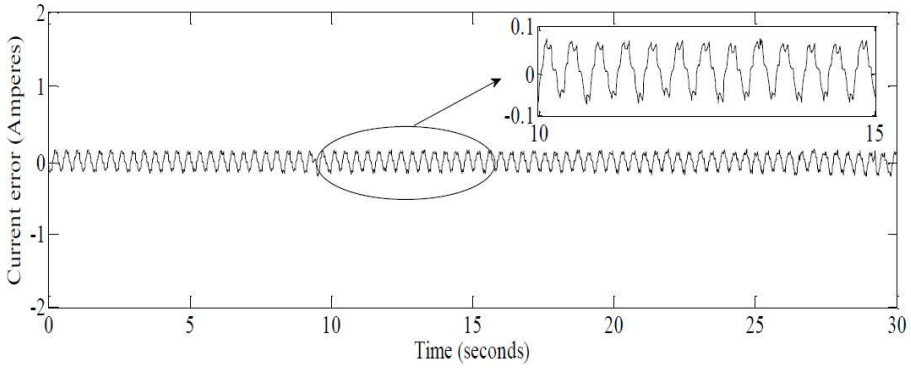

Figure 8. Experimental results of induction motor direct current error for the 2nd DOF

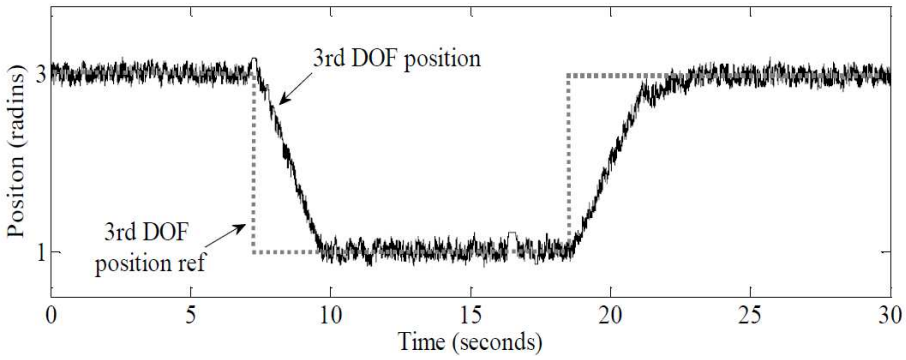

Figure 9. Experimental results of angular position of 3rd DOF

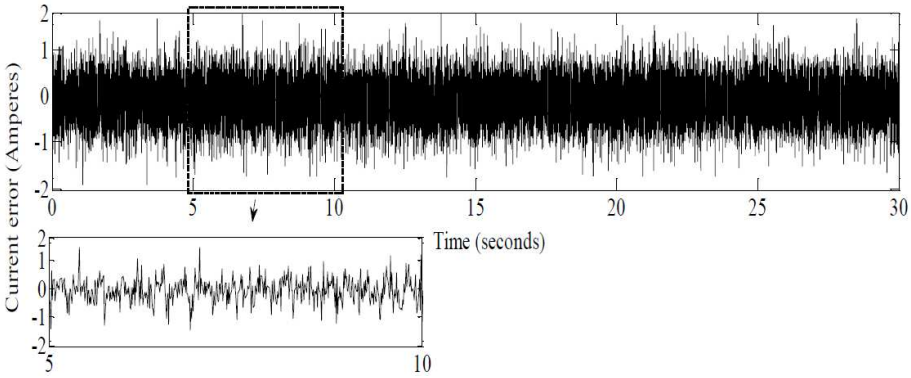

Figure 10. Experimental results of induction motor quadrature current error for the 3rd DOF

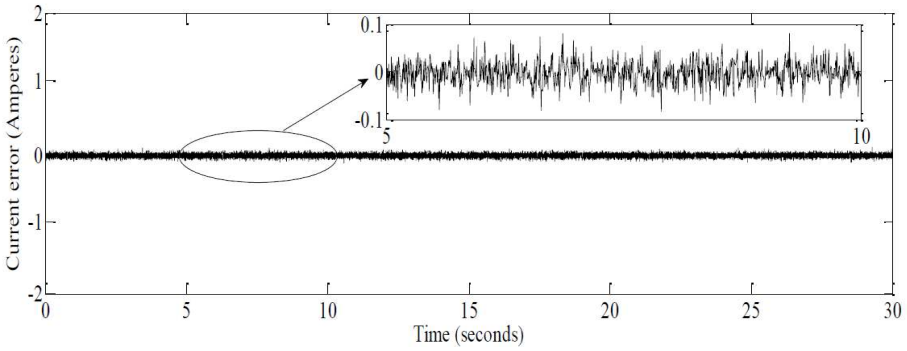

Figure 11. Experimental results of induction motor direct current error for 3rd DOF

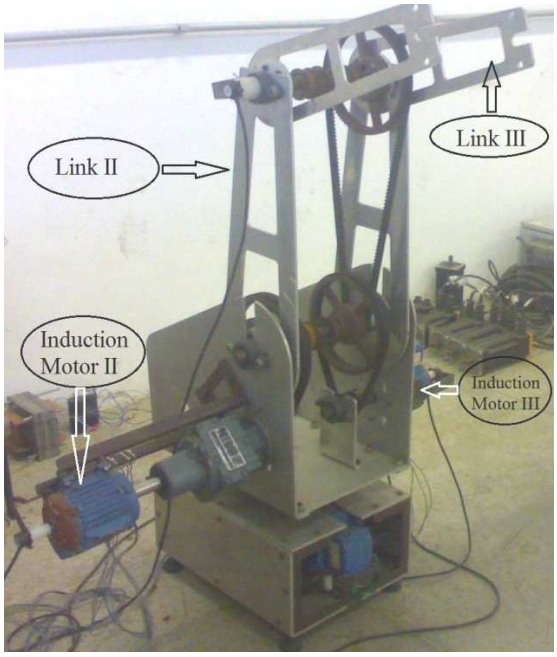

Figure 12. Three-link manipulator driven by induction motors

References

Aström K.J., Lee T.H., Tan K.K. and Johansson K.H. (1995) Recent Advances in Relay Feedback Methods-A Survey. *IEEE International Conference on Systems, Man and Cybernetics, Intelligent Systems for the 21st Century*, **3**, 2616–2621.

Blaschke F. (1971) The Principle of Field Orientation – the Basis for the Transvector Control of Three-Phase Machines. *Siemens Zeitschrift*, **3**(10): 757–760.

Bose B. K. (2001) *Modern Power Electronics and AC Drives*, 1st edition. Prentice-Hall PTR

Camara H. T., Carati E. G., Hey H. L., Pinheiro H., Pinheiro J. R. and Grundling H. A. (2003) Speed and Position Servo for Induction Motor using Robust Model Reference Adaptive Control. *IECON 28th Annual Conference of the Industrial Electronics Society* **2**: 779-787.

Casadei D., Profumo F., Serra G. and Tani A. (2002) FOC and DTC: Two Viable Schemes for Induction Motor Torque Control. *IEEE Transactions on Power Electronics* **17** (5): 177–185.

Chan C. C. and Wang H. Q. (1996) New Scheme of Sliding-Mode Control for High Performance Induction Motor Drives. *IEEE Proceedings in Electric Power Applications* **143** (3): 177–185.

Diniz E. C Júnior, Honório A. B. S., Almeida D. A. and Barreto L. H. S. C. (2010 a) Comparison Between Sliding Mode Control and Vector Control for a DSP-Based Position Control Applied to Squirrel-Cage Induction Motor. *9th IEEE/IAS International Conference on Industry Applications* **1**: 553–558.

Diniz E. C Júnior, Honório A. B. S., Almeida D. A. and Barreto L. H. S. C. (2010 b) Simplified Approach for Modelling and Control a 3-DOF RRR type Robotic Manipulator Using Squirrel-Cage Induction Motors. *9th IEEE/IAS International Conference on Industry Applications* **8**, 1–7.

Faa Jeng Lin, Po Kai Huang, Chou W.D. (2007) Recurrent Fuzzy Neural Network Controlled Linear Induction Motor Servo Drive Using Genetic Algorithms. *IEEE Transactions on Industrial Electronics* **3** (54): 1449–1461.

Gadoue S.M., Giaouris D. and Finch J.W.(2009) Sensorless Control of Induction Motor Drives at Very Low and Zero Speeds Using Neutral Network Flux Observers. *IEEE Transactions on Industrial Electronics* **56** (8): 3029–3039.

Gao W. and Hung J.C. (1993) Variable Structure Control Of Nonlinear Systems: A New Approach. *IEEE Transactions on Industrial Electronics* **49** (1): 45–55.

Holtz J.(1994) Pulse Width Modulation for Electronic Power Conversion. *IEEE Proceedings in Electronic Industrial Electronics* **82** (8):1194–1214.

Huh S.-H. and Bien Z. 1993) Robust Sliding mode Control of a Robot Manipulator Based on Variable Structure-Model Reference Adaptive Control Approach. *IET Control Theory & Applications* **1** (5):1355–1363.

Jussi P. (2006) Induction Motor Versus Permanent Magnet Synchronous Motor in Motion Control Applications: A Comparative Study. Department of Electrical Engineering. University of Lappeenranta, Lappeenranta, Finland.

Kumar R., Gupta R.A. and Bhangale S.V. (2009) Vector Control Techniques for Induction Motor Drive: A Review. *International Journal of Automation and Control* **3** (4): 284–306.

Novotny D. W. and Lipo T.A. (1996) *Vector Control and Dynamics of AC Drives*. 1st edition. Oxford University Press, New York.

Osama M. and Abdul-Azim O. (2008) Implementation and Performance Analysis of An Elevator Electric Motor Drive System. *12th International Middle-East Power System Conference* **5** (12):114–118.

Shiau L. G. and Lin J. L.(2001) Stability of Sliding-mode Current Control for High Performance Induction Motor Position Drives. *IEEE Proceedings in Electronic Power Applications* **148** (1): 69–75.

Spong M. W. and Vidyasagar M.(2004) *Robot Dynamics and Control*, 1st. edition. Wiley & Sons, Asia.

Szabat K., Orlowska-Kowalska T. and Dybkowski M.(2009) Indirect Adaptive Control of Induction Motor Drive System with an Elastic Coupling. *IEEE Proceedings in Electronic Industrial Electronics* **56** (10): 4038–4042.

Tomei P., Verrelli C. M., Montanari M. and Tilli A. (2009) Robust Output Feedback Learning Control for Induction Motor Servo Drives. *International Journal of Robust and Nonlinear Control* **15** (19):1745–1759.

Trzynadlowski A. M. (1982) *The Field Orientation Principle in Control of Induction Motors*, 1st edition. Springer.